ResearchGate

See discussions, stats, and author profiles for this publication at: http://www.researchgate.net/publication/280520759

CHARACTERIZATION AND MODELING OF THE STRAIN-RATE, TEMPERATURE AND PRESSURE DEPENDENCE OF THE DEFORMATION OF A HIGHLY CROSSLINKED AEROSPACE GRADE EPOXY RESIN

CONFERENCE PAPER · JULY 2015

CITATION
1

READS
75

4 AUTHORS:

Frédéric Lani
Université catholique de Louvain
39 PUBLICATIONS **363** CITATIONS
SEE PROFILE

Xavier Morelle
Université catholique de Louvain
7 PUBLICATIONS **3** CITATIONS
SEE PROFILE

Christian Bailly
Université catholique de Louvain
169 PUBLICATIONS **2,435** CITATIONS
SEE PROFILE

Thomas Pardoen
Université catholique de Louvain
231 PUBLICATIONS **3,941** CITATIONS
SEE PROFILE

All in-text references underlined in blue are linked to publications on ResearchGate, letting you access and read them immediately.

Available from: Frédéric Lani
Retrieved on: 23 November 2015

CHARACTERIZATION AND MODELING OF THE STRAIN-RATE, TEMPERATURE AND PRESSURE DEPENDENCE OF THE DEFORMATION OF A HIGHLY CROSSLINKED AEROSPACE GRADE EPOXY RESIN

Frédéric Lani[1], Xavier Morelle[1], Christian Bailly[2], Thomas Pardoen[1]

[1]Institute of Mechanics, Materials and Civil Engineering (IMMC), Université catholique de Louvain, Place Sainte-Barbe, n°2, L5.02.02, 1348 Louvain-la-Neuve, Belgium
Email: frederic.lani@uclouvain.be

[2]Institute of Condensed Matter and Nanosciences (IMCN), Université catholique de Louvain
Place L. Pasteur, n°1 L4.01.01, 1348 Louvain-la-Neuve, Belgium

Keywords: Epoxy resin, plasticity, strain rate, temperature, pressure, viscoplasticity

ABSTRACT

The non-linear behavior of the RTM6 aerospace grade epoxy resin is characterized and modeled by addressing the effects of strain-rate, temperature and hydrostatic pressure. The elastic-plastic constitutive model is based on a simple pressure dependent modified Von Mises yield criterion. A hardening function incorporating pre-upper yield non-linearity, softening and re-hardening is developed. Strain-rate and temperature dependences of the true stress-strain curve are introduced via the coefficients of the hardening function. The constitutive model is selected in order to be directly applicable with the standard distribution of the general purpose finite element software Abaqus, without the need for coding a user defined material subroutine. The introduction of the identified model in the current engineering practice is thus straightforward and will facilitate the use of the identified mechanical behavior of RTM6 in numerical multi-scale analyses of composites.

1 INTRODUCTION

Three key elements in the use of accurate experimental mechanical characterization of epoxy resins in the frame of multi-scale analyses reside in the availability of a constitutive model with a reasonable number of parameters which can be identified in a straightforward manner, in the robustness of implementation and in the simplicity of use in general purpose finite element simulation packages. In this context, the present work aims at proposing a simple constitutive model motivated by an in-depth analysis of the aerospace grade epoxy resin RTM6, partly inspired from the 'metal plasticity' culture. The proposed model combines the simplicity of an elastic-plastic model such as the one proposed by Hobbiebruken et al. [1], while incorporating the major physical principles of the mechanics of polymers (pressure-sensitivity, possible compressibility, strain-rate and temperature dependence through e.g. Eyring's law of transition of state [2], entropic resistance to chain alignment at large strains) which have been largely taken into account in the family of visco-plastic models originated from the pioneering work of e.g. Boyce [3] or Tervoort [4]. This contribution also addresses the modelling of the post peak yield behaviour, including softening and re-hardening, and, in this sense, goes one step beyond the experimental and modelling work by Gerlach et al. [5] on the mechanical behaviour of RTM6 under impact loads. Based on the experimental results presented in this paper and using the identified hardening behavior, a micromechanical failure criterion has been developed and identified – see the companion paper by Chevalier et al [6].

2 MATERIALS AND TESTING METHODS

2.1 Material

Hexflow RTM6, supplied by Hexcel, is a mono-component epoxy resin specifically developed to fulfill the requirements of aerospace and space industry in advanced RTM process. It is an amine-cured glassy thermoset composed of a premixed system of a tetra-functional epoxide precursor

(TGMDA) and a blend of two di-amine hardeners (MDEA and MMIPA). After curing, this aerospace qualified resin has a high glass transition temperature (Tg) around 220°C, thus providing high stiffness (E ~ 3 GPa at room temperature) and good thermal stability properties. A modified cure cycle has been developed in order to manufacture thick resin slabs while avoiding temperature overshoot problems in the specimen core due to the exothermal character of the crosslinking reaction.

The mechanical behaviour of the resin generally shows limited variability in a single batch, while batch to batch variability can be significant (5 to 15% difference in stress and modulus) due to different thermal history before, during and after curing.

2.2 Machining and mechanical testing

Cylindrical resin slabs were machined into small cylindrical specimens (12mm height by 12mm diameter) for uniaxial compression tests and into cylindrical dog bone specimens (either 6mm diameter by 36mm gauge length or 9mm diameter by 50mm gauge length) for the uniaxial tensile tests.

The tests were carried out on a screw-driven universal testing machine (Zwick-Roell with an external loading cell of 250 [kN]). These tests were performed either at constant true strain rate (CSR) or at constant crosshead displacement rate (CCDR) covering 4 decades of strain rates (between 10^{-4} s^{-1} and 0.1 s^{-1} for the CSR tests and between ~1.65 10^{-4} s^{-1} and ~0.165 s^{-1} for the CCDR tests). The behavior in tension has been characterized either at a constant true strain rate of 10^{-3} s^{-1} (CSR tests) or at a constant crosshead displacement rate of 1mm/min (CCDR tests). With the exception of the tensile tests at a constant true strain rate, all the tests were performed at three different temperatures: room temperature ~20°C (293K), 100°C (373K) and 150°C (423K).

For compression tests, Teflon strips were used as solid lubricant between the compression platens and the samples in order to minimize the barreling. Compared with any other liquid lubricant (e.g. grease oil), Teflon really allowed avoiding specimen barreling.

3 CONSTITUTIVE MODEL

The constitutive model is selected in order to be directly applicable with the standard distribution of the general purpose finite element software Abaqus [7], without the need for coding user defined material subroutines. The introduction of the identified model in the current engineering practice is thus straightforward.

The behavior of the material is assumed to be elastic-plastic. In its present formulation, the model is not intended for being used in the simulation of creep or relaxation. The dependence of the hardening behavior on the strain rate and temperature is given explicitely to Abaqus, which makes the model useful for simulating loading rate and temperature effects in the frame of quasi-static simulations (given a characteristic simulation time or loading history).

The selected yield criterion follows a linear Drucker-Prager [8] model, inspired from the ‘metal plasticity’ or ‘geo-materials’ cultures, which is a simple pressure dependent Mises yield surface. Isotropic hardening is assumed – i.e. no kinematic hardening is accounted for.

A hardening function incorporating pre-upper yield non-linearity, softening and re-hardening is developed. Strain-rate and temperature dependences of the true stress-strain curve are introduced via the coefficients of the hardening function. The strain-rate and temperature dependence of these coefficients can for instance be deduced from some principles of rubber elasticity or can be connected with thermally (and mechanically) activated segmental and macromolecular motion through the Eyring’s law of transition of states expressed for the effective plastic strain rate $\dot{p}$:

$$\dot{p} = \dot{p}_0 \exp\left(\frac{\sigma \Omega_A}{k_B T}\right) \exp\left(\frac{-\Delta G}{RT}\right)$$

where $\dot{p}_0$ is some reference transformation rate, σ is the applied stress, Ω_A is the apparent activation volume associated with the transformation, ΔG is the activation enthalpy associated with the transformation, k_B is the Boltzmann constant, R the gas constant and T the temperature.

3.1 Yield criterion

In polymers, the yield behavior is sensitive to the hydrostatic stress. This phenomenon is due to the different behavior of the free volume under tensile or compressive stresses (see e.g. [9]). A simple approach to the modeling of the yield behavior is to modify classical plasticity yield surfaces to account for the influence of hydrostatic stress. Modified Tresca or Von Mises yield surfaces are often proposed. Among them, pressure dependent yield surfaces like the Mohr-Coulomb and Drucker Prager models are often used for polymers.

In this paper, the original linear Drucker-Prager yield criterion is selected:

$$F = \sigma_e + \frac{\sigma_{mm}}{3}\tan(\beta) - \left(1 - \frac{\tan(\beta)}{3}\right)\sigma_c = 0$$

where σ_e is the Von Mises effective stress, σ_{mm} is the trace of the stress tensor, σ_c is the yield stress in compression. The term β is the friction angle, defined as

$$\tan(\beta) = 3\frac{1-r}{1+r}$$

with the so-called 'instantaneous uniaxial stress ratio'

$$r = \left|\frac{\sigma_t}{\sigma_c}\right|_p$$

where σ_t and σ_c are the uniaxial true stress in uniaxial tension and compression at an arbitrary uniaxial plastic deformation p. In this contribution, the asymmetry of yielding between tension and compression is simply expressed by the ratio of peak yield between uniaxial tension and uniaxial compression tests (i.e. $p = p_U$) even if they are obtained at slightly different plastic strains ($p_{U,c} \neq p_{U,t}$).

In the linear Drucker-Prager model implemented in Abaqus, no dependence of the hardening behavior on the stress-state is allowed (i.e. isotropic hardening). Hence the hardening behavior is taken from uniaxial compression tests.

Although some strain rate and/or temperature dependence of the friction angle cannot be excluded, it is not addressed in the present paper.

3.2 Flow rule

Beside the definition of the yield surface, yield is described by a flow rule. In this frame, the flow potential G is defined as

$$G = \sigma_e + \frac{\sigma_{mm}}{3}\tan(\varphi)$$

where φ is the 'so-called' dilation angle in the $(\sigma_e, -\frac{\sigma_{mm}}{3})$ plane. When $\varphi = \beta$, the incremental plastic strain vector is normal to the yield surface in the $(\sigma_e, -\frac{\sigma_{mm}}{3})$ plane and the plastic flow is associated with and derives from the yield criterion. When φ is different from β the flow is non-associated. When $\varphi = 0$, then plastic incompressibility is assumed. The non-associated flow rule might cause some convergence issues of the host finite element software when dealing with heterogeneous stress states.

The dilation angle at a given plastic strain p is computed as

$$\tan(\varphi) = -\frac{3(1-2v_p)}{2(1+v_p)}$$

where v_p^C is the plastic 'Poisson' coefficient measured in compression given by

$$v_p^C = \frac{p_r^c}{p_z^c}$$

with p_r and p_z the radial and axial plastic strains in an uniaxial compression test. The plastic strain tensor is given by

$$p_{ij} = \varepsilon_{ij} - S_{ijkl}\sigma_{kl}$$

where ε_{ij} is the strain tensor, σ_{kl} is the stress tensor, S_{ijkl} is the elastic compliance matrix of the resin.

Although some strain rate and/or temperature dependence of the dilation angle cannot be excluded, it is not addressed in the present paper. In its present formulation the Drucker-Prager model requires a single value of the dilation angle φ.

3.3 Elastic behavior

The resin is isotropic with Young's modulus *E* and Poisson ratio v. For the sake of simplicity, the Poisson ratio is taken as rate and temperature insensitive. The asymmetry of Young's modulus between tension and compression is neglected as a first approximation. The compression modulus is thus used. In line with [10] and [5] for what concerns the temperature and the strain rate dependences, respectively, the compression modulus is assumed to take the following form:

$$E(T,\ln(\dot{\varepsilon})) = \bar{E}(293)e^{(\beta_T(T-293))} + k_\varepsilon(\ln(\dot{\varepsilon}) - c_\varepsilon)$$

where $\bar{E}(293)$ is the compression modulus averaged over all strain rates at room temperature, c_ε is the average of the logarithms of all the tested true strain rates, β_T and k_ε are fitting parameters. The identified strain-rate dependence of the Young's modulus should hold up to strain rates of 100 s^{-1} [5]. In most quasi-static loading situations, the dependence on strain-rate could even be neglected.

3.4 Hardening behavior

The temperature and strain-rate dependent hardening behaviour is identified against the uniaxial compression experiments. It is assumed that the strain hardening does not depend on the stress triaxiality, which can be admitted as the resin is brittle in tension; however, in general, the re-hardening part can be highly sensitive to the hydrostatic stress. Hence, Poulain et al. [10] show that the hardening behaviour of their moderately crosslinked epoxy is different in tension and compression on the whole range of strain. Besides, the entropic resistance is known to be pressure dependent which is thus not accounted for in the model.

The hardening behaviour of the resin is described by a sum of three main contributions: the pre-peak hardening behaviour σ_A related with main chain segmental motion activation, the softening part σ_B coming from shear-transformation, localization combined with free volume rearrangement and then the re-hardening σ_C often referred to as the entropic spring contribution. This approach, illustrated in Figure 1, is inspired by the seminal work of Haward and Tackray [11].

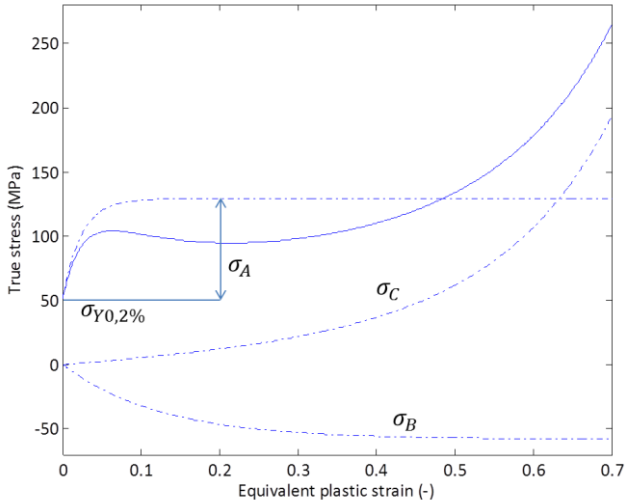

Figure 1. Decomposition of the compressive true stress-strain curve of RTM6 into three contributions : pre-peak hardening, softening and re-hardening.

The formulation presented here relies on the commonly accepted understanding of the molecular motion of entangled or cross-linked glassy polymers during straining. Below the glass transition temperature, in order to achieve large inelastic strain, the polymer has to overcome two main types of physical-mechanical resistance: the intermolecular resistance $(\sigma_{Y02} + \sigma_A + \sigma_B)$ and the entropic resistance $\sigma_{C_{11}}$.

At low strains, the polymer has to be stressed enough above the yield stress σ_{Y02} (and with an appropriate stress triaxiality) in order to exceed the activation energy for segment rotation (different types of segment rotations are involved, with different relaxation times). The contribution of this mechanism to the hardening of the polymer is denoted σ_A and has the following expression:

$$\sigma_A = \sigma_{A0}\left(1 - e^{-r_A p}\right)$$

where σ_{A0} is the targeted plateau stress and r_A is a fitting parameter driving the hardening rate.

As part of the stress-strain behaviour, significant softening is usually observed after the peak yield. Softening is due to shear transformation / large inter-molecular movement and can be either related to the localization of strain under the form of shear bands or more generally to any heterogeneity of stress which would simultaneously bring loading and unloading of distinct regions in the polymers, at a yet undefined length-scale. The contribution of this mechanism to the hardening of the polymer is denoted σ_B and writes:

$$\sigma_B = \sigma_{B0}\left(1 - e^{-r_B p}\right)$$

where σ_{B0} is the targeted plateau yield drop and r_B is a fitting parameter driving the softening rate.

At larger strains, the latest contribution is due to the entropic resistance to the alignment of the molecular network. This contribution is derived here from the Arruda & Boyce 8-chain model of rubber elasticity [12]:

$$\boldsymbol{\sigma}_C = \frac{C_R}{3}\frac{\sqrt{N}}{\lambda_p}\mathcal{L}^{-1}\left(\frac{\lambda_p}{\sqrt{N}}\right)dev(\mathbf{B})$$

where C_R is the hardening modulus (C_R is the rubbery modulus for material in the rubbery state), $\sqrt{N}$ the limiting chain extensibility, $\mathbf{B} = \mathbf{F}\mathbf{F}^T$ is the left Cauchy-Green tensor and $dev(\mathbf{B})$ its deviator,

with $\mathbf{F}$ the plastic deformation gradient (note: in the following expression, plastic incompressibility is assumed)

$$\mathbf{F} = \begin{pmatrix} e^{p_{11}} & 0 & 0 \\ 0 & e^{p_{22}} & 0 \\ 0 & 0 & e^{p_{33}} \end{pmatrix} = \begin{pmatrix} e^{p_{11}} & 0 & 0 \\ 0 & e^{-0.5p_{11}} & 0 \\ 0 & 0 & e^{-0.5p_{11}} \end{pmatrix} = \begin{pmatrix} e^{p} & 0 & 0 \\ 0 & e^{-0.5p} & 0 \\ 0 & 0 & e^{-0.5p} \end{pmatrix}.$$

The term λ_p is the stretch on a chain of the 8-chain network defined as

$$\lambda_p = \sqrt{\frac{trace(\mathbf{B})}{3}} \quad .$$

The symbol $\mathcal{L}^{-1}$ represents the inverse Langevin function, which is here approximated by the explicit function

$$\mathcal{L}^{-1}(x) \approx 3\frac{3-x^2}{1-x^2} \quad .$$

Other expressions for the re-hardening could be assumed, considering for instance a Neo-Hookean behaviour, a 3-chain or 8-chain model or the approximated full-chain model by Wu and Van der Giessen [13]. Note that entropic springs such as the 8-chain model detailed in the expression of $\boldsymbol{\sigma}_C$ imply the existence of transverse stresses that should be iteratively removed by applying an appropriate transverse strain in order to recover a pure uniaxial test; the present model overlooks this effect by just taking into account the axial component of $\boldsymbol{\sigma}_C$. First, the impact of neglecting the transverse stresses brought by the entropic spring is that the identified parameters will be slightly different. Second, considering the spring as a simple hardening function relating the effective stress and the equivalent plastic strain cancels its 'multi-axial contribution' and inherent pressure-sensitivity.

The compression stress of the resin can then be expressed as

$$\sigma \quad = \sigma_{Y02} + \sigma_{A0}(1 - e^{-r_A p}) + \sigma_{B0}(1 - e^{-r_B p}) + \sigma_{C_{11}}$$

where $\sigma_{C_{11}}$ is the axial component of the re-hardening stress.

The strain-rate and temperature dependence of the stress parameters $\sigma_{Y02}, \sigma_{A0}$ is assumed to follow the inverted Eyring's equation, i.e.

$$\sigma_i = \frac{k_B T}{\Omega_{A_i}}\left(\ln(\dot{p}) - \ln(\dot{p}_{0_I})\right) + \frac{\Delta G_i}{N_A \Omega_{A_i}}$$

with *i = Y02* or *i = A0;* N_A is the Avogadro number. Inspired by the work of Boyce in [3] where the saturation stress is taken as a constant fraction of the so-called 'athermal shear strength', the strain rate and temperature dependence of σ_{B0} is introduced through $\sigma_{B0} = -k\,\sigma_U$ where *k* is a strain-rate and temperature insensitive fitting parameter named 'yield drop coefficient' while σ_U is the strain-rate and temperature dependent peak yield stress, which also obeys the inverted Eyring's equation. The parameter r_A governing the pre-peak hardening rate is taken as

$$r_A = r_{A,a} T^{n_A} + r_{A,b}$$

while r_B, the parameter governing the softening rate, is kept constant.

In line with the approach of Arruda et al. [14], C_R is assumed independent of strain rate and temperature. Then $\sqrt{N}$ is taken independent of strain-rate while its sensitivity to temperature is expressed as

$$N(T) = \frac{n(293)N(293)}{B_h + A_h\left(1 - e^{-\frac{E_h}{k_B T}}\right)}$$

where $n(T)$ is the chain density at temperature T, E_h is the thermal dissociation energy and A_h and B_h are fitting parameters. This last expression expresses the fact that the number of efficient rigid links per chain $n(T)N(T)$ remains constant whatever the temperature. Alternately, for materials below the glass transition temperature, Rottler [15] reports that the hardening modulus C_R should depend linearly on the lower yield stress (having by consequence the same strain-rate and temperature sensitivities) and on the hydrostatic pressure.

Table 1 summarizes the parameters that must be identified, some of them can be identified directly from the experimental results, while other are identified through a procedure of global fitting of the stress strain curves. The minimum set of experiments must involve 4 compression tests (e.g. 2 tests at different constant true strain rates and room temperature, and 2 tests at different temperatures, whatever the selected strain rate) and one tensile test at room temperature and at a constant true strain rate (for which a RT compression test is available).

	Parameters
Modulus parameters	$\beta_T\ k_\varepsilon\ \bar{E}(293)\ c_\varepsilon$
Poisson ratio	v
Stress ratio	r
Plastic Poisson ratio	v_p^C
Activation volumes	$\Omega_{A_U}\ \Omega_{A_{Y02}}\ \Omega_{A_{A0}}$
Activation enthalpies	$\Delta G_U\ \Delta G_{Y02}\ \Delta G_{A0}$
Reference transformation rates	$\dot{p}_{0_U}\ \dot{p}_{0_{Y02}}\dot{p}_{0_{A0}}$
Yield drop coefficient	k
Hardening kinetics coefficients	$r_{A,a}\ r_{A,b}\ n_A\ r_B$
Rubbery modulus	C_R
Efficient chain segments	$A_h\ B_h\ E_h\ N(293)$

Table 1.

4 RESULTS AND DISCUSSION

4.1 Experimental results

Note: in this document stress and strain refer to true stress and true strain.

Compression and tensile tests results at constant true strain rate and constant crosshead displacement rate are shown in Figure 2 and Figure 3, respectively. Not all but only representative true stress-strain curves are shown in these figures.

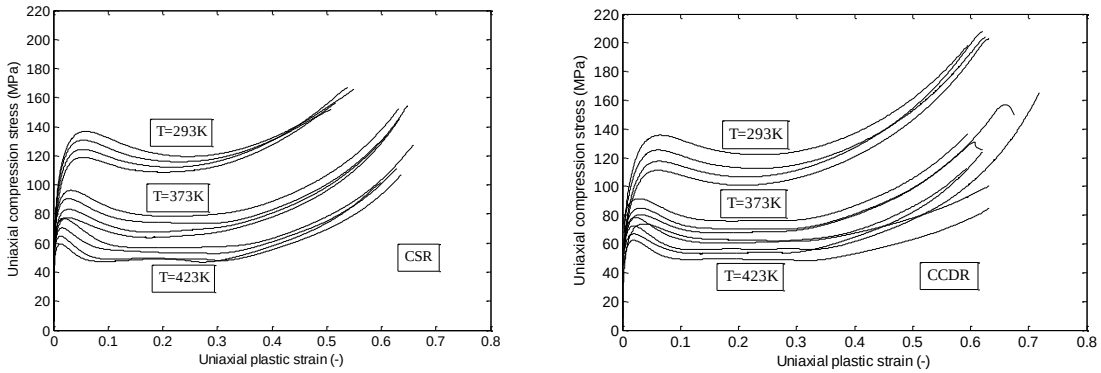

Figure 2. Experimental results. Left: compression tests at constant true strain rate (from 10^{-4} to 10^{-1} 1/s) and right: constant crosshead displacement rate (from 0.1 to 100mm/min) for three temperatures (293K, 373K, 423K).

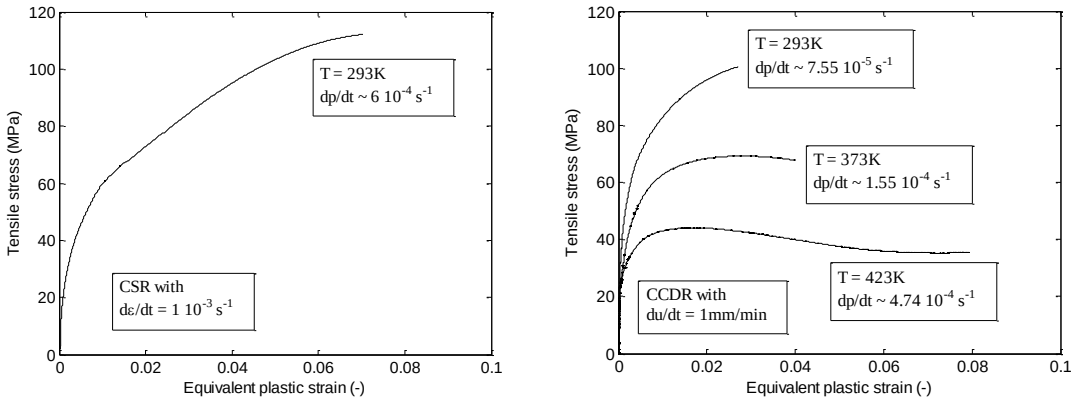

Figure 3. Experimental results. Left: tensile tests at constant true strain rate (10^{-3} 1/s) and room temperature and right: tensile tests at constant crosshead displacement rate (1 mm/min) for three temperatures (293K, 373K, 423K).

The compressive and tensile CSR tests were made with the same batch of resin. The CCDR compressive and tensile tests were performed with samples coming from different batches, but without samples coming from the 'CSR batch'.

The following points must be highlighted:

- batch to batch variability of modulus and peak yield stress of up to 15% can be observed,
- the compressive plastic strain at failure looks rather insensitive to temperature and strain rate, and close to 0.6, except for the RT tests at a constant true strain rate. However, there is a significant difference between the tests performed at RT at a constant true strain rate or at a constant crosshead rate: there is about a 50MPa and a 0.1 drop of the failure stress and plastic strain at failure respectively for the constant true strain rate tests. No other explanation than the batch/operator variability can be given to explain this difference;
- only the tensile and compression tests performed at the same constant true strain rates can be directly exploited to extract the asymmetry of yielding at peak yield between tension and compression. In order to exploit the CCDR tests, the peak yield in compression must first be deduced using the identified Eyring fit using the average plastic strain rate of the investigated corresponding tensile test. Then the ratio of peak yield is computed between a real peak yield in tension and a virtual peak yield obtained from the Eyring fit.
- the tensile tests perfomed at room temperature and constant true strain rate and constant crosshead speed bring slightly different pre-peak hardening behaviors of the resin at low strains. No other explanation than the batch/operator variability can be given to explain this

difference. Furthermore the tensile curves at room temperature do not actually reach the peak yield. However, for one of them the slope of the curve at failure is so close to zero that the failure stress is assumed to be equal to the peak yield.

4.2 Parameters identification

The identification is made here with the CSR tests only.
The identification of the model parameters is made through a two-step procedure:

1. Several model parameters (13) can be identified directly against the experimental results: the modulus parameters (β_T k_T, $\bar{E}(293)$, c_ε), the Poisson ratio v, the stress ratio r, the plastic Poisson ratio v_p^C, the stress parameters σ_{Y02} and σ_U (activation volumes, enthalpies and reference transformation rates that appear in the inverted Eyring's equation).
2. The remaining model parameters (13) are identified by minimizing the distance between the predicted compression true stress-strain curves and the remarkable experimental couples shown in Figure 4. Additionally the slope of the stress strain curve should be zero at the peak yield and lower yield. A gradient based optimizer provided in Matlab [16] is used for that purpose.

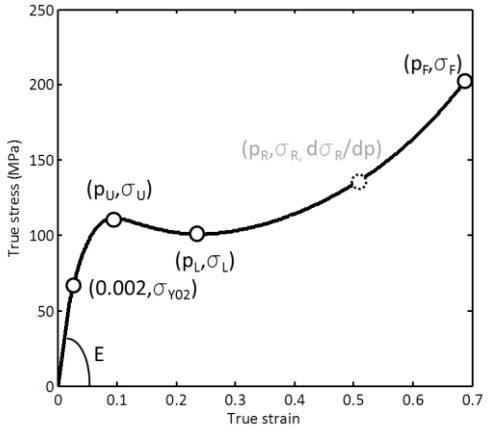

Figure 4. Remarkable (plastic strain, stress) couples used for parameter identification.

The parameters identified using the aforementioned procedure are listed in Table 2.

β_T	k_ε	$\bar{E}(293)$	c_ε	v	r	v_p^C	Ω_{A_U}	$\Omega_{A_{Y02}}$	$\Omega_{A_{A0}}$
1/K	MPa s	MPa	1/s	-	-	-	mm^3	mm^3	mm^3
-0.00261	30.64	2587	-5.86	0.38	0.912	~0.5	$1.8\ 10^{-18}$	$3.8\ 10^{-18}$	$2.6\ 10^{-18}$

ΔG_U	ΔG_{Y02}	ΔG_{A0}	$\dot{p}_{0_U}$	$\dot{p}_{0_{Y02}}$	$\dot{p}_{0_{AO}}$	k	$r_{A,a}$	$r_{A,b}$	n_A	r_B
J/mol	J/mol	J/mol	1/s	1/s	1/s	-	1/K	-	-	-
$2.86\ 10^5$	$2.06\ 10^5$	$4.76\ 10^5$	$2.83\ 10^{23}$	$3.04\ 10^7$	$8.79\ 10^{49}$	0.954	8526	43.4	4.65	1.536

C_R	A_h	B_h	E_h	$N(293)$
MPa	-	-	J/mol	-
22.5	$1.19\ 10^{36}$	$9\ 10^{32}$	5.4	1.81

Table 2.

The identified activation volumes are in the same range as those reported in [17] for a DGEBA epoxy resin. The main parameters of the re-hardening part (C_R, $N(293)$) are also comparable with values reported in the literature for other glassy polymers. The resulting true stress-strain curves are shown in Figure 5.b, with representative experimental results reproduced in Figure 5.a for the sake of comparison. A good agreement is found in terms of capability to reproduce the hardening behavior in

the given range of strain rates and temperature. As shown in Figure 6.a, the model is also capable of predicting the behavior in tension however discrepancies are observed at low plastic strains as the pre-peak hardening behavior was shown to be different in tension and compression. The tensile curves predicted at the other temperatures (with the average strain rates computed from the CCDR tests) are shown in Figure 6.b. While the behavior is well predicted at room temperature, this figure suggests that the pressure sensitivity of yielding is temperature dependent as well.

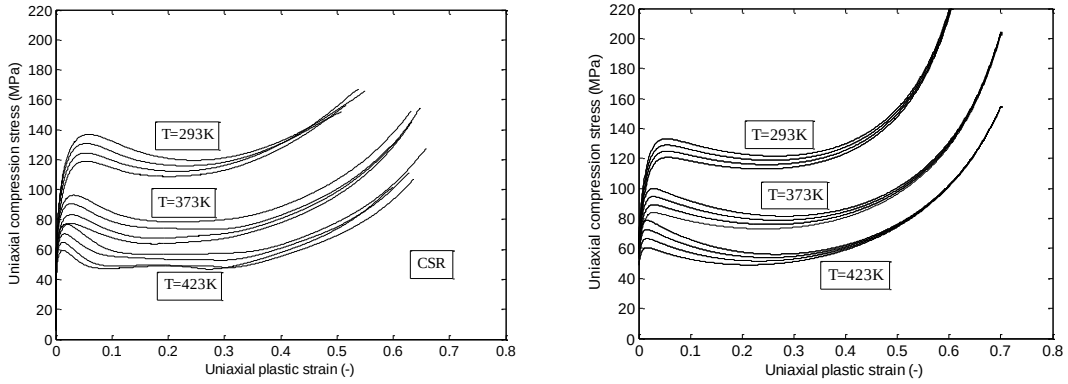

Figure 5. a) experimental true stress - true strain curves for RTM6 from compression tests; b) responses identified by the present model. Note that the curves predicted by the model are arbitrarily interrupted at a plastic strain of 0.7 as failure is not addressed in this paper.

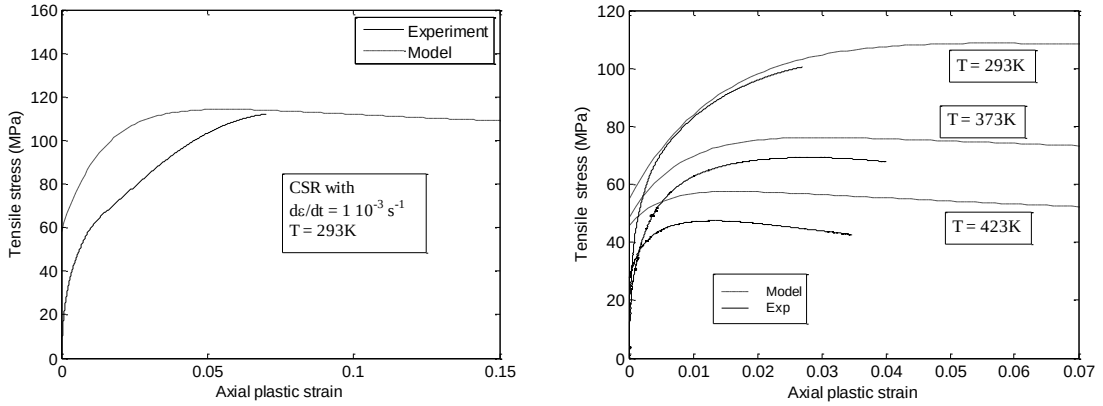

Figure 6. Comparison of model predictions and experimental responses in tension: a) tensile true stress-true strain curve at a constant true strain rate; b) tensile true stress-true strain curves at a constant crosshead displacement rate.

5 CONCLUSION

The proposed hardening law associated with the linear Drucker-Prager yield surface and non-associative flow rule is capable to reproduce the sensitivity to strain rate, temperature and hydrostatic pressure of the non-linear deformation behavior of a thermoset polymer. It has been identified for an important aerospace grade epoxy system, namely the RTM6 resin. It has been used in a companion paper to identify a micromechanical failure criterion [6] for the resin. The model can now be used as a key ingredient in the multi-scale analysis of the deformation and failure of composites under monotoneous loadings without the need for implementing a user-defined material subroutine. Hence the identified model paramaters can be used readily in the standard distribution of the general purpose finite element software Abaqus. Current limitations of the model include the fact that it cannot reproduce the back stress observed upon unloading, it cannot be used to simulate creep of relaxation experiments, it cannot handle the apparent temperature dependence of the pressure-sensitivity of yielding. Ongoing parallel research intended to circumvent these limitations is presented by V.-D. Nguyen et al. who develop a large strain constitutive model for amorphous glassy polymers and

assess it against experimental results for the same RTM6 epoxy resin.

REFERENCES

[1] Thomas Hobbiebrunken, Bodo Fiedler, Masaki Hojo, Shojiro Ochiai, Karl Schulte, Microscopic yielding of CF/epoxy composites and the effect on the formation of thermal residual stresses, Composites Science and Technology, 65(10), 1626-1635 (2005)

[2] Eyring, Henry, Viscosity, plasticity, and diffusion as examples of absolute reaction rates, The Journal of Chemical Physics, 4, 283-295 (1936)

[3] Mary C. Boyce, David M. Parks, Ali S. Argon, Large inelastic deformation of glassy polymers. part I: rate dependent constitutive model, Mechanics of Materials, 7(1), 15-33 (1988)

[4] Tervoort, T. A. and Klompen, E. T. J. and Govaert, L. E., A multi-mode approach to finite, three-dimensional, nonlinear viscoelastic behavior of polymer glasses, Journal of Rheology (1978-present), 40, 779-797 (1996)

[5] Robert Gerlach, Clive R. Siviour, Nik Petrinic, Jens Wiegand, Experimental characterisation and constitutive modelling of RTM-6 resin under impact loading, Polymer, 49(11), 2728-2737 (2008)

[6] J. Chevalier, X. Morelle, C. Bailly, T. Pardoen, F. Lani, Micro-mechanical modeling of the pressure dependent failure of a highly crosslinked epoxy resin, 20th Conference on Composite Materials ICCM20, Copenhagen, 19-24 July 2015

[7] Abaqus v6.12, General purpose finite element software, Dassault Systèmes

[8] Drucker, D. C. and Prager, W., Soil mechanics and plastic analysis for limit design. Quarterly of Applied Mathematics, 10(2), 157–165 (1952)

[9] T.F. Guo, J. Faleskog, C.F. Shih, Continuum modelling of a porous solid with pressure-sensitive dilatant matrix, Journal of the Mechanics and Physics of Solids, 56, 2188–2212 (2008)

[10] X. Poulain, A.A. Benzerga, R.K. Goldberg, Finite-strain elasto-viscoplastic behavior of an epoxy resin: Experiments and modeling in the glassy regime, International Journal of Plasticity, 62, 138-161 (2014)

[11] R. N. Haward , G. Thackray, The Use of a Mathematical Model to Describe Isothermal Stress-Strain Curves in Glassy Thermoplastics, Proc. R. Soc. Lond. A, 302, 453-472 (1968)

[12] Arruda, E. M. and Boyce, M. C., A three-dimensional model for the large stretch behavior of rubber elastic materials,, J. Mech. Phys. Solids, 41(2), 389–412 (1993)

[13] P.D. Wu, E. Van Der Giessen, On improved network models for rubber elasticity and their applications to orientation hardening in glassy polymers, Journal of the Mechanics and Physics of Solids, 41(3), 427-456 (1993)

[14] Ellen M. Arruda, Mary C. Boyce, R. Jayachandran, Effects of strain rate, temperature and thermomechanical coupling on the finite strain deformation of glassy polymers, Mechanics of Materials, 19(2–3), 193-212 (1995)

[15] J. Rottler, Fracture in glassy polymers: a molecular modeling perspective, Journal of Physics: Condensed Matter, 21(46), 1-17 (2009)

[16] MATLAB Release 2012b, The MathWorks, Inc., Natick, Massachusetts, United States.

[17] T. Gomez-del Rio, J. Rodriguez, Compression yielding of epoxy: strain rate and temperature effect, Materials and Design, 35, 369-373 (2012)

[18] V.-D. Nguyen, X. Morelle, F. Lani, T. Pardoen, C. Bailly, L. Noëls, An elastoplastic-damage constitutive model based on a large strain hyperelastic formulation for amorphous glassy polymers, 20th Conference on Composite Materials ICCM20, Copenhagen, 19-24 July 2015